An Integrated Design and Control Optimization Framework for Hybrid Military Vehicle Using Lithium-Ion Battery and Supercapacitor as Energy Storage Devices

Abdullah-Al Mamun, Zifan Liu, Denise M. Rizzo, and Simona Onori, *Senior Member, IEEE*

***Abstract*— One of the existing challenges toward the electrification of military vehicles is the selection of the most suitable energy storage device. Moreover, a single energy storage technology might not provide the most benefit out of powertrain electrification. In this paper, a generalized framework for the simultaneous selection of the optimal energy storage device, in the form of a standalone or hybrid solution, and online energy management is presented. This paper investigates the cooperation of energy-dense Li-ion batteries and power-dense supercapacitors to assist engine operation in a series hybrid electric military truck. Pontryagin's minimum principle is adopted as the energy management strategy in a forward-looking vehicle simulator, in which the optimal design and control parameters are found using particle swarm optimization. Simulation results show that adopting a hybrid energy storage system reduces fuel consumption by 13% compared to the case of battery-only hybridized powertrain.**

***Index Terms*— Design optimization, energy management, Li-ion battery, portraying's minimum principle (PMP), supercapacitor (SC).**

I. Introduction

THANKS to its significant fuel saving potential, the powertrain hybridization technology is finding the path into different vehicle classes, from light-duty passenger vehicles to heavy-duty military trucks [1]. In military applications, hybridization of the powertrain can provide the increased tactical capability of military vehicles by increasing the available onboard power, along with reducing the battlefield fuel costs [2], [3].

There are various energy storage system (ESS) candidates for the alternative energy sources in hybrid electric vehicles (HEVs). Li-ion battery technology is the most commonly used device for electrified propulsion systems, nowadays, due to its higher power and energy density and declining cost [4]. In addition, the power to propel the vehicle can be further supplemented by adding other ESSs [5].

Supercapacitors (SCs) have higher power density compared to the Li-ion battery allowing effective regeneration when the battery cannot operate in the regenerative mode [5]. The high pulse power capability, fast transient response, and high efficiency during charge and discharge cycles make SCs a viable ESS choice to be used in conjunction with Li-ion batteries in a hybrid ESS (HESS) configuration [6], [7]. This will also have positive implications on battery aging as the high-power density storage, i.e., the SC can handle the demanded power spikes [8], [9].

In the context of this paper, besides an internal combustion engine as the primary mover, a HESS pack consisting of Li-ion battery and SC is considered in the HEV under study. Proper sizing and power management of such a HESS have the potential to reduce lifecycle cost and weight of the storage system while improving the fuel economy.

In [10], an HESS pack with battery and SC is designed for an electric bus. The battery pack size is determined with the required minimal electric range, and dynamic programming (DP) is used to find the SC pack size that minimizes the life cycle cost. In [11], for an HESS pack in a fuel cell HEV, the power rating of each energy storage device is scaled up or down to quantitatively assess the significance of appropriate sizing on system volume/mass and battery lifetime. In [12], applications of HESS, such as smart grid and HEV using design optimization techniques, including genetic algorithm (GA), particle swarm optimization (PSO), and simulated annealing are presented. The above-mentioned studies look only at optimizing the size of the HESS for given rule-based energy management strategies. In contrast, many studies focus on developing control strategies for a given ESS size to achieve certain control objectives, such as minimizing fuel consumption, battery degradation, and so on. Those strategies can be categorized into heuristic, near-optimal, and optimal ones. Heuristic strategies are usually rule based [13], [14] and low-pass filter based [15], [16]. Despite their straightforward implementation, a large number of calibration efforts are required. Optimal control strategies include DP [17], [18],

Manuscript received June 15, 2018; revised August 23, 2018; accepted August 28, 2018. Date of publication September 6, 2018; date of current version March 19, 2019. This work was supported by the ARC at the University of Michigan under Cooperative Agreement W56HZV-14-2-0001 with the U.S. Army Tank Automotive Research, Development, and Engineering Center, Warren, MI, USA. *(Corresponding author: Simona Onori.)*

A.-A. Mamun and Z. Liu are with the Department of Automotive Engineering, Clemson University, Greenville, SC 29607 USA (e-mail: amamu@clemson.edu; zifanl@clemson.edu).

D. M. Rizzo is with the U.S. Army Tank Automotive Research, Development, and Engineering Center, Warren, MI USA (e-mail: denise.m.rizzo2.civ@mail.mil).

S. Onori is with the Department of Energy Resources Engineering, Stanford University, Stanford, CA 94305 USA (e-mail: sonori@stanford.edu).

Digital Object Identifier 10.1109/TTE.2018.2869038

Pontryagin's minimum principle (PMP), and equivalent consumption minimization strategy (ECMS) [19], [20]. They generate optimal control sequence with *a priori* information of the drive cycle and set the optimal performance benchmark, making themselves suitable for offline applications. For online implementation, near-optimal EMS strategies can be used to pursue the best achievable system efficiency. The model predictive control [5], [21] and adaptive PMP/ECMS [22] have been discussed for HEV with HESS. They require adaptive tuning of a set of parameters to meet varying real-world power demands. However, to explore the full potential of an HESS configuration in an HEV, the component sizing and energy management should be optimized in an integrated manner.

Combined design optimization and energy management are often solved in a layered approach. In [23], the GA and rule-based EMS were used to simultaneously optimize the monetary cost and the fuel economy of an HEV with a fuel cell, battery, and SC. The power and state-of-charge (SOC) limits of the rules and the pack sizes are optimized simultaneously. Masih-Tehrani *et al.* [24] minimize the monetary cost and battery degradation for an HEV with engine and battery and SC. In the outer loop, GA iterates across the design space for optimal sizing parameters, while in the inner loop, DP searches for optimal control sequences. The design and control parameters are sought iteratively in a two-layer framework. Convex programing recently arises as an effective approach to tackle the HESS design and control problem bringing less computational burden if compared with DP [25], [26]. However, a large number of model simplifications into convex forms are needed which may neglect important vehicle and component dynamics. The investigation in [27] introduced the coupling of GA and ECMS for multiobjective optimization of an HEV with the engine, battery, and SC. A multicriteria decision-making technique is used to choose among the solutions with conflicting goals. From this method, it is often difficult to understand the impact of design and control variables on a specific objective which is of principal importance, such as fuel consumption of military vehicles.

The above-mentioned literature presents the benefits of using HESS configuration which motivates this paper to further explore the combined design optimization and energy management of HESS for military vehicle hybridization. However, a rigorous mathematical formulation and solution approach that is computationally efficient and general enough for a wide range of ESSs and powertrain configurations are still missing in the existing literature. This paper lays the foundation of a new optimization framework that simultaneously accounts for both the control and design variables of a hybrid or electric vehicle powertrain. This paper specifically develops an approach using PMP and PSO for combined design optimization and energy management of an HESS in an HEV to minimize fuel consumption over a given drive cycle.

The proposed solution method pursued in this paper is based on the construction of the Hamiltonian function defined in a way to include both sizing (number of Li-ion cells and number of SC cells) and control (power split among the engine, the battery pack, and the SC pack) variables. The proposed optimization approach also allows the inclusion of additional optimization objectives which might be important for different vehicle types and classes. In the proposed framework, we allow one of the costates of the PMP to dynamically vary over time. Therefore, the proposed optimization framework can be extended to plug-in HEV (PHEV) design and energy management where the assumption of a constant costate does not hold [28]. To the best of our knowledge, this is the first work that formulates such a generalized and combined design and control optimization framework that is applicable across a wide range of vehicle classes and also across a wide range of electrification choices.

Fig. 1. M-ATV [29].

This paper is organized as follows. The models of the vehicle, the battery, the SC, and other components are introduced in Section II. The PMP, the PSO, and their integrated formulation are discussed in Section III. Next, five military drive cycles are used under the integrated optimization framework to find the ESS sizing and energy management strategy across different driving conditions, and results are presented in Section IV. Conclusions and future work are outlined in Section V.

II. Model Description

This paper uses a notional series hybrid version of a mine-resistant ambush-protected all-terrain vehicle (M-ATV), as shown in Fig. 1 [29]. A powertrain model of the series hybrid M-ATV, obtained from [30], comprises a generator set (genset, Navistar 6.4L 260-kW diesel engine + 265-kW generator), four 95-kW brushless permanent magnet direct current in-hub motors, and a lithium iron phosphate (LFP) battery pack. In the battery pack, the number of LFP cells in series ($N_{s,\mathrm{Li}}$) is 130 and the number of cells in parallel ($N_{P,\mathrm{Li}}$) is 10. The genset and the battery pack are connected to the power bus which provides electric power to the four in-hub motors. The vehicle simulator is set up in a Simulink environment where a PID controller is used as a driver model to find the required propulsion power by minimizing the vehicle speed following error. Longitudinal dynamics equations are used in the simulator to simulate the vehicle motion and the genset, and the motors are represented by their quasi-static efficiency maps. Details of the vehicle simulator can be found in [30]. The vehicle simulator has a feedforward fuel control logic which is removed to reduce the number of tuning parameters.

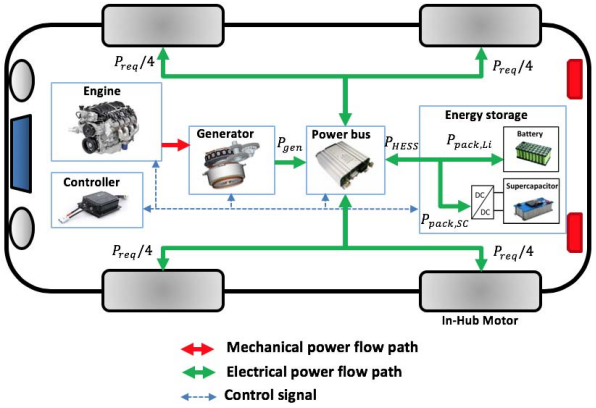

Fig. 2. SHEV architecture where the total power demanded by the four in-hub motors is supplied by the genset and the HESS pack including an NMC Li-ion battery pack and a SC pack.

The performance of the obtained HEV simulator in terms of fuel consumption without the feedforward fuel control is considered as the baseline against which the solution of the proposed optimization algorithm is compared. A low-pass filter-based EMS is used in this simulator to split the power between the genset and the battery pack. Since the existing EMS is not optimized, in our previous work [31], we have implemented an optimal control strategy to obtain the benchmark solution in terms of power split and optimal battery size where the nickel manganese cobalt (NMC) battery chemistry is used instead of LFP.

To further explore the benefit of hybridization using more than one ESS, in this paper, we have considered an HESS configuration including an NMC Li-ion battery pack and a SC pack. A semiactive configuration is utilized in the HESS configuration where the SC pack is connected to the power bus through a dc–dc converter as shown in Fig. 2. The optimal control strategy splits the total power required by the four in-hub motors, $P_{\text{req}}(t)$ into power demanded from the battery pack $P_{\text{pack,Li}}(t)$, the SC pack $P_{\text{pack,SC}}(t)$, and the genset $P_{\text{gen}}(t)$.

A. Lithium-Ion Battery Model

In the HESS configuration, the electrical behavior of the NMC battery pack is modeled by a first-order equivalent circuit model (ECM) whose parameters are temperature dependent. Fig. 3(a) shows the circuit diagram, where E_o represents the open circuit voltage (OCV) of the cell, which is a function of the cell SOC, and I_{cell} is the input current (positive in discharge).

The series resistance R_0 captures the internal loss of the cell including the current collector. The RC pair, with a resistance R_1 and capacitance C_1, captures the diffusion dynamics of the cell. The equations of the battery ECM are

$$\dot{V}_{C_1} = -\frac{V_{C_1}}{R_1 C_1} + \frac{I_{\text{cell}}}{C_1} \tag{1}$$

$$\dot{\text{SOC}} = -\frac{I_{\text{cell}}}{Q_{\text{nom}}} \tag{2}$$

$$V_{\text{cell}} = E_o - R_0 I_{\text{cell}} - V_{C_1} \tag{3}$$

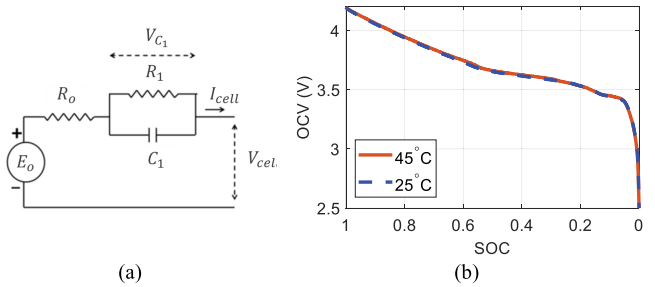

Fig. 3. (a) First-order equivalent circuit model used to model the dynamic behavior of NMC Li-ion battery. (b) Measured OPV of the NMC Li-ion cell as a function of the state of charge under a temperature of 23 °C and 45 °C [31].

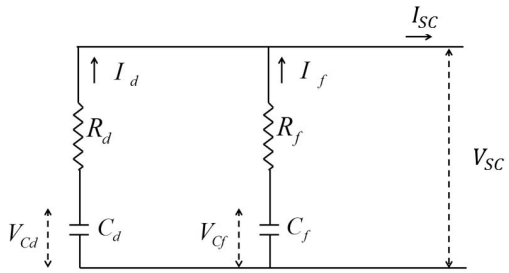

Fig. 4. Second-order SC equivalent circuit model.

where Q_{nom} is the nominal capacity of the cell, and (3) provides the relationship for the voltage response of the cell, V_{cell} as a function of the model parameters and input, I_{cell}. The parameters (R_0, R_1, C_1) in the above-mentioned model are assumed to be functions of SOC, temperature, and current directionality (charge versus discharge). Data collected from capacity and hybrid pulse power characterization tests performed at the Battery Aging and Characterization Laboratory at Clemson University were used to identify the parameters [31].

A two-state thermal model for Li-ion borrowed from [32] is used in this paper to capture the dynamic temperature variation of the NMC Li-ion cell during charge and discharge. Parameters of the thermal model description of the model equations, model parameter identification, and validation are provided in [31].

B. Supercapacitor Model

The SC cell is modeled in this paper by a second-order ECM consisting of two capacitor–resistor branches similar to that in [33], as shown in Fig. 4. The $R_f C_f$ branch captures the fast dynamics of the order of few seconds and the $R_d C_d$ branch captures the delayed dynamics of minutes.

The equations comprising the electrical model are as follows:

$$\dot{V}_{Cf} = \frac{I_f}{C_f} \tag{4}$$

$$\dot{V}_{Cd} = \frac{I_d}{C_d} \tag{5}$$

$$I_{\text{SC}} = I_f + I_d \tag{6}$$

$$V_{\text{SC}} = I_f R_f + V_{Cf} = I_d R_d + V_{Cd} \tag{7}$$

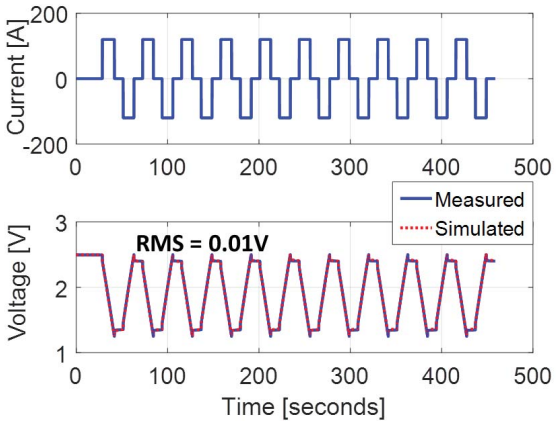

Fig. 5. For the input current in the top plot, the SC cell voltage is measured and used to fit the ECM model. Calculated RMS error shows that the identified model captures the voltage response with an RMS of 10 mV.

TABLE I
ELECTRICAL AND THERMAL PARAMETERS OF BCAP1500 SC CELL

Parameters	Values
R_f (Ω)	0.0015
C_f (F)	1430
R_d (Ω)	2.2067
C_d (F)	2224
h_{SC} (W/K)	1.516
C_{SC} (J/K)	235.24

where C_f and C_d are the capacitances of the capacitors in the fast and delayed dynamics branches, and V_{Cf} and V_{Cd} are the corresponding voltages across the capacitors. The resistances of the fast and delayed dynamics branches are R_f and R_d. The currents flowing into the fast and delayed branches are I_f and I_d, respectively; positive current during charge is assumed. The terminal voltage and current through the system terminals are denoted as $V_{\rm SC}$ and $I_{\rm SC}$, respectively.

A first-order thermal model is used to capture the SC temperature change during charge and discharge

$$C_{\rm SC}\dot{T}_{\rm SC} = I_{\rm SC}^2 R_f - h_{\rm SC}(T_{\rm SC} - T_{\rm amb}) \tag{8}$$

where $C_{\rm SC}$ is the heat capacity of the cell, $T_{\rm SC}$ is the core temperature, and $h_{\rm SC}$ is the effective heat transfer coefficient of a cell. The parameters of a BCAP1500 SC [34] are identified from a pulse current profile and shown in Fig. 5. The comparison of the model terminal voltage with the measured terminal voltage is also shown in Fig. 5.

The identified electrothermal model parameters are compiled in Table I.

C. DC–DC Converter Model

In this paper, the SC pack is connected in parallel to the power bus through a bidirectional dc–dc converter in a semiactive configuration, as shown in Fig. 6. A dc–dc converter takes

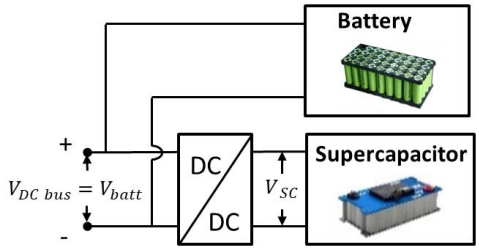

Fig. 6. Input and output voltages of a switching dc–dc converter.

an unregulated voltage as the input and produces a regulated output voltage by means of pulse-width modulation [35]. The dc–dc converter works in two distinct modes: "buck" and "boost" mode. In this paper, the dc–dc converter is used for voltage conversion between the dc bus and the SC during charge and discharge of the SC. The mode of operation of the dc–dc converter changes due to: 1) change in the direction of SC power flow, $P_{\rm SC}$, during charge and discharge and 2) the difference between the SC pack voltage, $V_{\rm SC}$, and the dc bus voltage, $V_{\rm batt}$. Table II shows the equivalent circuit models of the dc–dc converter in different operating modes. In a real system, the single-pole double-throw switch shown in the circuits of Table II, is realized by semiconductor devices such as MOSFETS, diodes, and so on. The inductor L and the capacitor C form a low-pass filter which allows only the dc component of the input voltage to pass through. The internal loss in the dc–dc converter is modeled by assuming a resistance (R_L) of the inductor winding L. The voltage conversion is achieved through high-frequency switching between position 1 and position 2 and by generating a rectangular wave form. During switching, the fraction of the time the switch is in position 1, which determines the output voltage and is defined as the duty cycle. Duty cycle for the buck mode ($0 \leq D_{\rm buck} \leq 1$) and the boost mode ($0 \leq D_{\rm boost} \leq 1$) is different due to their direction of conversion [35].

Table II also shows four different settings under which the dc–dc converter is operated when used in the HESS configuration. During discharge of the SC, $P_{\rm SC} > 0$, the SC voltage $V_{\rm SC}$ is the input terminal voltage of the dc–dc converter and the dc bus voltage $V_{\rm batt}$ is the output terminal voltage. In that case, if SC voltage is higher than the dc bus voltage ($V_{\rm SC} > V_{\rm batt}$), the converter operates in the buck mode. On the other hand, if the SC voltage is lower than dc bus voltage ($V_{\rm SC} > V_{\rm batt}$), the converter operates in the boost mode. A similar condition arises when the SC pack is charged through power coming from the dc bus. In that case, the dc bus voltage $V_{\rm batt}$ is the input terminal voltage of the dc–dc converter and the SC voltage $V_{\rm SC}$ is the output terminal voltage. Similar to discharging, two conditions arise during charging given the relative magnitude of voltage in the input and terminal output of the converter. Power losses during voltage conversion affect the conversion efficiency of the dc–dc converter, which is a function of the internal resistance R_L of the converter, the duty cycle, and the resistance of the output terminal, determining the final converter efficiency. Since the output terminal changes upon the direction of current, the efficiency

TABLE II

EQUATIONS OF THE VOLTAGE CONVERSION RATIO AND EFFICIENCY FOR THE BIDIRECTIONAL BUCK–BOOST DC–DC CONVERTER UNDER DIFFERENT OPERATING CONDITIONS [35]

If $P_{SC} > 0$		
If $V_{SC} < V_{batt}$	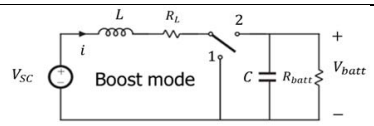	
	$\frac{V_{batt}}{V_{SC}} = \frac{1}{(1-D_{boost})\left(1+\frac{R_L}{(1-D_{boost})^2 R_{batt}}\right)}$	(9)
	$\eta = \frac{P_{out}}{P_{in}} = \frac{1}{1+\frac{R_L}{(1-D_{boost})^2 R_{batt}}}$	(10)
If $V_{SC} > V_{batt}$	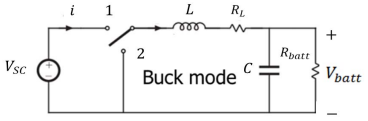	
	$\frac{V_{batt}}{V_{SC}} = \frac{D_{buck}}{1+\frac{R_L}{D_{buck} R_{batt}}}$	(11)
	$\eta = \frac{P_{out}}{P_{in}} = \frac{1}{1+\frac{R_L}{D_{buck} R_{batt}}}$	(12)
If $P_{SC} < 0$		
If $V_{batt} > V_{SC}$	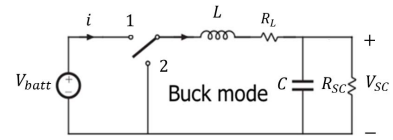	
	$\frac{V_{SC}}{V_{batt}} = \frac{D_{buck}}{1+\frac{R_L}{D_{buck} R_{SC}}}$	(13)
	$\eta = \frac{P_{out}}{P_{in}} = \frac{1}{1+\frac{R_L}{D_{buck} R_{SC}}}$	(14)
If $V_{batt} < V_{SC}$	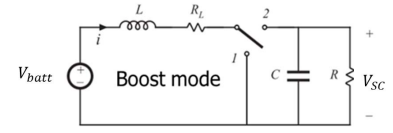	
	$\frac{V_{SC}}{V_{batt}} = \frac{1}{(1-D_{boost})\left(1+\frac{R_L}{(1-D_{boost})^2 R_{SC}}\right)}$	(15)
	$\eta = \frac{P_{out}}{P_{in}} = \frac{1}{1+\frac{R_L}{(1-D_{boost})^2 R_{SC}}}$	(16)

of the converter depends on the battery pack resistance, R_{batt}, during the boost mode and SC pack resistance, R_{SC}, in the buck mode.

For each mode in Table II, first, the voltage conversion ratio is found by dividing the output terminal voltage by the input terminal voltage [35]. The efficiency is computed as the ratio of power at the output terminal and the input terminal of the dc–dc converter. Expanding the equation of power and

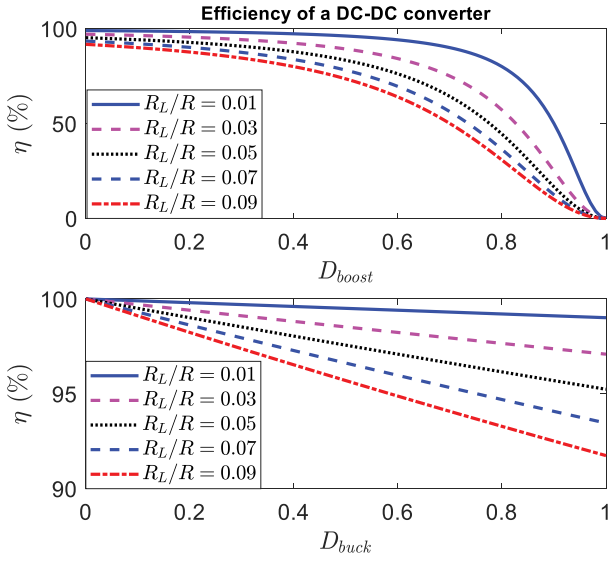

Fig. 7. Conversion efficiency plot under (a) boost and (b) buck modes of a dc–dc converter [38]. During discharge of the SC, $R = R_{\text{batt}}$, and during charging of SC, $R = R_{\text{SC}}$.

using the voltage conversion ratio, the expression of efficiency is obtained as a function of duty cycle, internal resistance, and resistance of the output terminal of the dc–dc converter $\eta(R_L, D_{\text{boost}}/D_{\text{buck}}, R_{\text{batt}}, R_{\text{sc}})$. The efficiency characteristics in the buck and boost modes are plotted in Fig. 7 as a function of duty cycle and ratio of resistances (R_L/R) where R is either R_{SC} or R_{batt} depending on the direction of current. Since the converter efficiency vary significantly with the duty cycle and resistance of the output terminal, it is important to take the efficiency calculation into account when designing an HESS configuration [35]. In this paper, a commercial SIEMENS SINAMICS DCP 120-kW dc–dc converter is chosen to be used with the SC pack. The internal resistance of the converter, which is attributed to the inductor resistance, R_L, is assumed to be 0.01 Ω [36]. The manufacturer limits on voltage, current, and power of the dc–dc converter are listed in [37].

III. PROBLEM FORMULATION AND SOLUTION APPROACH

The goal of this paper is to develop a generalized design optimization and energy management framework for a military HEV equipped with an HESS. The traditional approach to such a problem is to use a layered approach, where typically an exhaustive search algorithm is used in the outer layer to select the design parameters, whereas an energy management algorithm is designed in the inner layer by either borrowing tools from optimal control theory or through some heuristics/rule-based strategy. Such a two-layer iterative process can lead to unpractical computational time and complexity. This paper formulates a combined design optimization and energy management problem and outlines a solution approach that relies on the construction of the Hamiltonian function that integrates both design and control variables. The optimality of the Hamiltonian function can be ensured by enforcing the necessary conditions using PMP.

The goal is to minimize the overall fuel consumption, J, over a given drive cycle within the time horizon $[0,\ t_f]$

$$J = \int_0^{t_f} \dot{m}_{\text{fuel}}(P_{\text{gen}})dt \tag{17}$$

where $\dot{m}_{\text{fuel}}$ is the engine fuel consumption rate (kg/s) and P_{gen} is the power delivered by the engine-genset. The total electrical power required by the motors is

$$\begin{aligned} P_{\text{req}}(t) &= P_{\text{gen}}(t) + P_{\text{HESS}} \\ &= P_{\text{gen}}(t) + P_{\text{pack,Li}}(t) + P_{\text{pack,sc}}(t) \end{aligned} \tag{18}$$

where $P_{\text{pack,Li}}(t)$ and $P_{\text{pack,sc}}(t)$ are the battery pack power and SC pack power, respectively.

The total fuel consumption J can be expressed as a function of power delivered from the battery pack $P_{\text{pack,Li}}(t)$ and the SC pack $P_{\text{pack,sc}}(t)$ to supplement the genset power $P_{\text{gen}}(t)$ at each time instant as

$$J = \int_0^{t_f} \dot{m}_{\text{fuel}}(P_{\text{pack, Li}}(t) + P_{\text{pack,SC}}(t))dt. \tag{19}$$

Assuming homogeneity in the packs, the battery pack power in (19) can be expressed as a product of the number of Li-ion cells in series ($N_{s,\text{Li}}$), the number of Li-ion cells in parallel ($N_{p,\text{Li}}$), and the power delivered by a single Li-ion cell $[P_{\text{cell, Li}}(t)]$. Similarly, the SC pack power can be expressed as a product of the number of SCs in series ($N_{s,\text{SC}}$), the number of SCs in parallel ($N_{p,\text{SC}}$), and the power delivered by a single SC cell $[P_{\text{cell, SC}}(t)]$. Using these relationships in (19), one obtains

$$\begin{aligned} J = \int_0^{t_f} \dot{m}_{\text{fuel}}(N_{s,\text{Li}} \cdot N_{p,\text{Li}} \cdot P_{\text{cell,Li}}(t) + N_{s,\text{SC}} \cdot N_{p,\text{SC}} \\ \cdot P_{\text{cell,SC}}(t))dt. \end{aligned} \tag{20}$$

In this paper, it is assumed that the number of Li-ion cells in series is known and found by dividing the dc bus voltage with a nominal voltage of an NMC Li-ion cell. The above-mentioned cost function is constrained by the system states.

In the supervisory controller module, a simpler model of the Li-ion battery and SC is used to reduce computational complexity. A zero-order model of the Li-ion battery and a first-order model for the SC are used, where the voltage across the capacitor of the delayed dynamics branch is the only state of the SC.

In the following generalized formulation, the battery SOC is indicated as $x_1(t)$ and the voltage across the capacitor of the delayed dynamics branch V_{Cd} in the SC model is indicated as $x_2(t)$. The HESS state vector is then defined as $\boldsymbol{x}(t) = [x_1(t)\ x_2(t)]$, where

$$\begin{aligned} \dot{x}_1(t) &= -\frac{I_{\text{pack,Li}}(t)}{Q_{\text{pack}}} \\ &= -\frac{I_{\text{cell,sc}}(t)}{Q_{\text{nom}}} = \frac{E_0 - \sqrt{E_0^2 - 4R_0 P_{\text{cell,Li}}(t)}}{2R_0 Q_{\text{nom}}} \end{aligned} \tag{21}$$

$$\begin{aligned} \dot{x}_2(t) &= -\frac{I_{\text{pack,sc}}(t)}{C_{\text{d,pack}}} = -\frac{I_{\text{cell,sc}}(t) \cdot N_{s,\text{sc}}}{C_d} \\ &= \frac{\left(V_{Cd} - \sqrt{V_{Cd}^2 - 4R_d P_{\text{cell,SC}}(t)}\right) \cdot N_{s,\text{sc}}}{2R_d C_d}. \end{aligned} \tag{22}$$

The HESS design variable vector is indicated as $\boldsymbol{v} = [N_{p,\text{Li}}\ N_{s,\text{sc}}\ N_{p,\text{sc}}]^T$. The control variables are the instantanious power from a single Li-ion cell and SC cell, $\boldsymbol{u}(t) = [u_1(t)\ u_2(t)]^T = [P_{\text{cell,Li}}(t)\ P_{\text{cell,SC}}(t)]^T$. The admissible set of design and control variables is defined as $\boldsymbol{V} = [\boldsymbol{v}_{\min}\ \boldsymbol{v}_{\max}]^T$ and $\boldsymbol{U}(t) = [\boldsymbol{u}_{\min}(t)\ \boldsymbol{u}_{\max}(t)]^T$, respectively. The goal of the optimization problem is to find the admissible design and control variables $\boldsymbol{\pi} \in \boldsymbol{\Pi} = [\boldsymbol{U}(t)\ \boldsymbol{V}]$

$$\boldsymbol{\pi}(t) = \begin{cases} \boldsymbol{u}(t) \in \boldsymbol{U}(t) \\ \boldsymbol{v} \in \boldsymbol{V} \end{cases} \tag{23}$$

such that

$$J = \int_0^{t_f} \dot{m}_{\text{fuel}}\left(\boldsymbol{\pi}(t)\right) dt \tag{24}$$

is minimized while subjected to (21), (22), and

$$\begin{aligned} \boldsymbol{v}_{\min} &\le \boldsymbol{v} \le \boldsymbol{v}_{\max} \\ \boldsymbol{x}(t_f) - \boldsymbol{x}(t_o) &= \Delta \boldsymbol{x} = 0 \\ \boldsymbol{u}_{\min}(t) &\le \boldsymbol{u}(t) \le \boldsymbol{u}_{\max}(t) \\ \boldsymbol{x}_{\min}(t) &\le \boldsymbol{x}(t) \le \boldsymbol{x}_{\max}(t) \\ T_{y,\min} &\le T_y(t) \le T_{y,\max} \\ \omega_{y,\min} &\le \omega_y(t) \le \omega_{y,\max} \\ y &= \text{engine, motor, generator.} \end{aligned}$$

Based on the above-mentioned problem formulation, a solution method is proposed where the Hamiltonian function is constructed in such a way that both design and control variables are included. PMP is a powerful tool that provides a set of necessary conditions of optimality in terms of the Hamiltonian function. The optimality is guaranteed by selecting the optimal control candidate that produces the lowest total cost.

The PMP has been successfully used in the literature to solve the optimal power split problem in HEVs [39]. In this paper, given the cost function (17), the Hamiltonian function is defined as follows:

$$\begin{aligned} &H(t, \boldsymbol{x}(t), \boldsymbol{\lambda}(t), \boldsymbol{u}(t), \boldsymbol{v}) \\ &\quad = \dot{m}_{\text{fuel}}(\boldsymbol{u}(t), \boldsymbol{v}) + \boldsymbol{\lambda}(t)^T \cdot \boldsymbol{f}(t, \boldsymbol{x}(t), \boldsymbol{u}(t), \boldsymbol{v}) \end{aligned} \tag{25}$$

where $\boldsymbol{f}$ is the vector of the state dynamics in (21) and (22) and $\boldsymbol{\lambda}(t)$ is the vector of costates, e.g., $\boldsymbol{\lambda}(t) = [\lambda_1(t)\ \lambda_2(t)]^T$ carrying the units of kilograms, equivalent to the amount of fuel saved thanks to the utilization of energy storage devices. Furthermore, the costates variables act as penalty on the energy storage devices usage: a higher value of $\boldsymbol{\lambda}(t)$ discourages the controller to use the available energy in the battery and the SC pack, whereas a low value assigned to the costates signifies that the usage of the battery/SC is preferred (in the sense that is cheaper) to the use of the ICE. The necessary conditions for optimality are the following:

1) *State Dynamics*:

$$\dot{x}_1(t) = \frac{\partial H}{\partial \lambda_1} = \frac{E_0 - \sqrt{E_0^2 - 4R_0 u_1(t)}}{2R_0 Q_{\text{nom}}} \tag{26}$$

$$\dot{x}_2(t) = \frac{\partial H}{\partial \lambda_2} = \frac{V_{Cd} - \sqrt{V_{Cd}^2 - 4R_d u_1(t)}}{2R_d C_d}. \tag{27}$$

2) *Costate Dynamics*:

$$\dot{\lambda}_1(t) = -\lambda_1 \frac{\partial H}{\partial x_1} = -\lambda_1 \frac{\partial}{\partial x_1}\left(\frac{E_0 - \sqrt{E_0^2 - 4R_0 u_1(t)}}{2R_0 Q_{\text{nom}}}\right) \tag{28}$$

$$\dot{\lambda}_2(t) = -\lambda_2 \frac{\partial H}{\partial x_2} = -\lambda_2 \frac{\partial}{\partial x_2} \times \left(\frac{\left(V_{Cd} - \sqrt{V_{Cd}^2 - 4R_d u_2(t)}\right) \cdot N_{s,\text{sc}}}{2R_d C_d}\right). \tag{29}$$

3) *Charge Sustainability*:

$$\boldsymbol{x}(t_f) - \boldsymbol{x}(t_o) = \Delta \boldsymbol{x} = 0. \tag{30}$$

4) *Optimality*:

$$H(t, \boldsymbol{x}^*(t), \boldsymbol{\lambda}^*(t), \boldsymbol{\pi}(t)) \geq H(t, \boldsymbol{x}^*(t), \boldsymbol{\lambda}^*(t), \boldsymbol{\pi}^*(t)). \tag{31}$$

The optimal solution $\boldsymbol{\pi}^*(t)$ is such that

$$\boldsymbol{\pi}^*(t) = \underset{\boldsymbol{\pi}(t) \in \boldsymbol{\Pi}(t)}{\text{argmin}} \; H(t, \boldsymbol{x}(t), \boldsymbol{\lambda}(t), \boldsymbol{\pi}^*(t)). \tag{32}$$

In HEV charge sustaining operation, SOC is usually constrained within a narrow window, within which, the OCV E_0 and the resistance R_0 can be assumed constant, thus making $\dot{x}_1(t)$ depend only on battery power $u_1(t)$. Therefore, from (28), $\lambda_1(t)$ is an unknown constant [5]. However, the same assumption cannot be applied to SC since the equation of costate is an explicit function of the state $x_2(t)$.

A. Implementation Methodology

To carry out the simultaneous design and control optimization, a PSO technique is chosen and integrated within a PMP framework to optimize both the design variables (ESSs sizing) and the control variables (power-split decision). When minimizing the Hamiltonian function in (25), the value of costates must be optimally tuned to achieve charge sustainability, and in the PSO algorithm, the constant costate corresponding to the Li-ion pack (λ_1) and the initial value of the dynamic costate corresponding to the SC pack ($\lambda_2(0)$) are treated as the control variables. To find the optimal set of design and control variables ($N^*_{p,\text{Li}}$, $N^*_{s,\text{SC}}$, $N^*_{p,\text{SC}}$, λ^*_1, $\lambda^*_2(0)$), first, the upper and lower limits for all variables are specified. The inbuilt *particleswarm* function in MATLAB is used in this paper, where each particle comprises a vector of variables randomly generated within the limits. The particles are evaluated by running the vehicle simulator over a designated drive cycle, and the Hamiltonian function is minimized at every time step, and the power split among the engine, battery pack, and SC pack is found along with the overall fuel consumption. The particles are then evaluated based on the overall fuel consumption. The process is repeated until a certain number of iterations are completed or until the change of the objective function is very small in subsequent iterations. The flow chart of the overall process is described in Fig. 8. The use of PSO instead of the widely used GA arises from the fact that PSO outperforms the GA in terms of computational efficiency [40]. The bounds are found based on the design constraints of the vehicle and preliminary assessment of the impact of the costate on charge sustainability. In this paper, it is assumed that the battery pack is directly connected to the vehicle power bus, and the dc bus voltage is the same as the battery pack voltage. From this assumption, the total number of NMC Li-ion cells in series is found to be 116 and used as a known design parameter.[1] The optimization algorithm is then designed to search for an HESS configuration where the energy capacity of the battery pack can vary over a wide range, roughly from 12% to 110% of the energy capacity of the original battery pack of the baseline vehicle. Given the number of cells in series as 116%, 12%, and 110% of the energy capacity of the baseline corresponds to a parallel string length ranging from 1 to 13 cells, respectively. On the other hand, the bounds on SC pack size are selected from the ability of the dc–dc converter to convert voltage with high conversion efficiency. In Fig. 7, one can see that the conversion efficiency is lower in the boost mode than that in the buck mode. Therefore, considering only the boost mode efficiency for finding a suitable range of SC pack size is sufficient to ensure the desired efficiency in the buck mode. In this paper, it is assumed that the efficiency of the dc–dc converter should not fall below 80%. From this

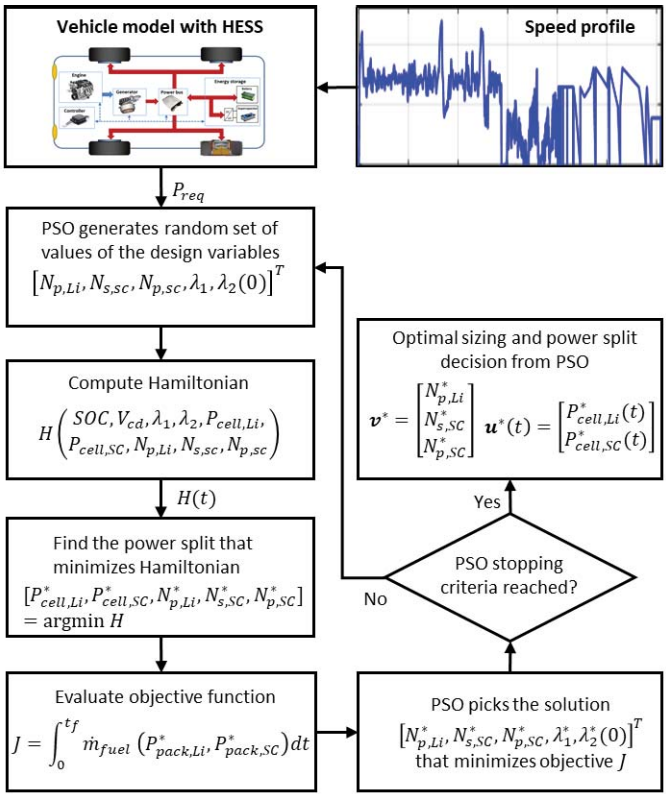

Fig. 8. Flow chart to solve the combined design optimization and energy management problem using an integrated approach based on PSO and PMP.

[1]The number of cells in a series string is found by dividing the dc bus voltage (429 V) by the nominal cell voltage of an NMC Li-ion cell.

assumption, the minimum number and maximum number of SC cells are obtained as

$$V_{\text{min,dc/dc}} \leq N_{S,\text{SC}} \cdot \eta_{\text{dc-dc,min}} \cdot V_{\text{SC,nominal}} \leq V_{\text{dc bus}} \tag{33}$$

where $V_{\text{min,dc/dc}}$ is the minimum voltage of the SC pack that the dc–dc converter can convert, $\eta_{\text{dc-dc,min}}$ is the minimum required efficiency of the dc–dc converter, $V_{\text{SC,nominal}}$ is the nominal voltage of the SC, and $V_{\text{dc bus}}$ is the dc power bus voltage. The minimum required efficiency of the dc–dc converter is selected to be 80% in this paper. From the above-mentioned inequality, the relationship for the bound on the number of SC cells in series is found as follows:

$$\frac{V_{\text{min,dc/dc}}}{\eta_{\text{dc-dc,min}} V_{\text{SC,nominal}}} \leq N_{S,\text{SC}} \leq \frac{V_{\text{ess}}}{\eta_{\text{dc-dc,min}} V_{\text{SC,nominal}}} \tag{34}$$

which gives the following numerical bounds:

$$42 \leq N_{S,\text{SC}} \leq 199. \tag{35}$$

In the optimization algorithm, the SC cells in parallel are allowed to vary between 1 and 15 based on the maximum discharge current limit of the dc–dc converter.

In order to account for the vehicle weight augmentation from the various ESS configurations, the algorithm updates the weight at each iteration/combination. In the baseline vehicle simulator, a lumped weight for the 26 650 LFP Li-ion cells, housing, power electronics, and cooling systems is used. Since the weight of an 18 650-NMC cell and SC cell varies significantly compared to an LFP cell, the weight of the individual NMC and SC cells is first obtained from the manufacturers' datasheet, and then 40%[2] increase in weight is added to account for the housing and other components of the pack [34].

The optimal power management strategy designed in this paper utilizes the ESSs under certain operating conditions. For example, in the propulsion mode, the battery can only be discharged, wherein in the braking mode, both charge and discharge are allowed. In the propulsion mode, the SCs can be charged or discharged and they can get charged from the engine only. As a result, all the battery power goes to meet the vehicle power requirements. This condition ensures that the SC has enough charge to supply any instantaneous power requirement when necessary. To ensure drivability and smooth engine operation, the allowable rate of change of engine power demand is limited to 80 kW/sec. During braking, the kinetic energy first goes to charge the SC and after that to the battery pack. This is a reasonable condition since the SC can be charged and discharged at a much faster rate than the battery pack.

IV. Simulation Results

In this section, the optimization problem to find the optimal size of HESS and the corresponding energy management is solved for the notional heavy-duty M-ATV military truck.

[2]The weight of the selected NMC Li-ion cell and the SC cell is 46 and 280 g, respectively.

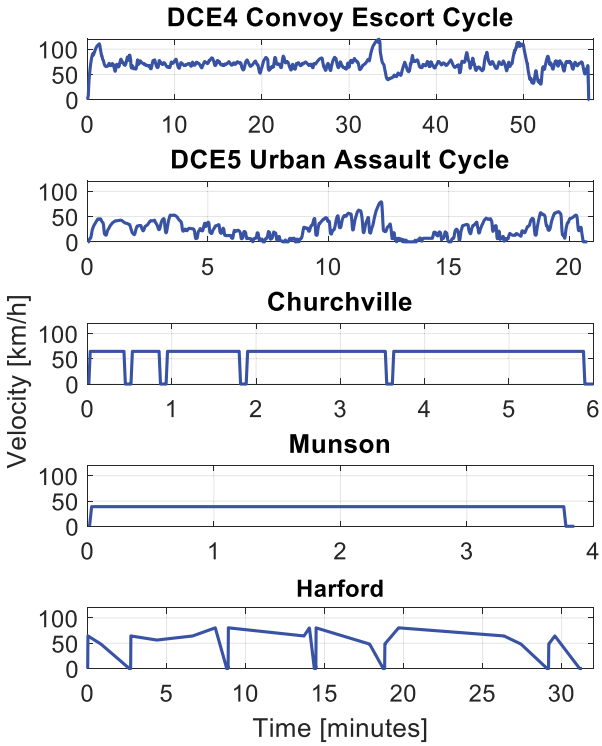

Fig. 9. Five military drive cycles used to evaluate the performance of the design optimization and energy management solution proposed in this paper.

The results are compared with the baseline vehicle simulator in terms of fuel consumption [30]. In addition, a battery-only ESS configuration with the NMC battery pack, studied in [31], is used for comparative analysis with both the HESS and baseline configurations. The optimization framework is implemented under five military drive cycles. The DCE4 Convoy Escort, DCE5 Urban Assault, Churchville, Munson, and Harford drive cycles [41], as shown in Fig. 9. The DCE5 cycle mainly describes a low-speed driving scenario with frequent acceleration and braking; the DCE4 cycle instead involves high-speed driving activities. Churchville and Harford cycles often require sharp acceleration and braking, whereas the Munson cycle describes a medium constant speed cruising activity. Churchville and Munson drive cycles are courses at the Aberdeen Proving Ground in Aberdeen, Maryland, while the other three are synthetic cycles.

A. Lithium-Ion Battery-Only Configuration

Before implementing the HESS configuration, it is important to assess and quantify the benefits of vehicle hybridization brought by an optimized battery-only ESS configuration developed in [31]. In this paper, the combined design and control optimization algorithm is run over a concatenated cycle made of the five military cycles (shown in Fig. 9) with the decision variables being the number of cells in series N_s, the number of cells in parallel N_p, and the battery costate λ.

The battery pack design and fuel consumption for the baseline and the optimized battery-only configuration are listed in Table III. The table shows that the optimized design and control policy can reduce the fuel consumption by 7.3%

TABLE III

COMPARISON OF THE BASELINE LFP PACK, THE OPTIMIZED NMC BATTERY PACK, AND THE HESS CONFIGURATIONS IN TERMS OF THE NUMBER OF CELLS, ENERGY CAPACITY, AND FUEL CONSUMPTION

	Size of the battery and the supercapacitor pack				**Energy capacity (kWh)**		**Fuel Consumption (L/100km)**
	$N_{s,Li}$	$N_{p,Li}$	$N_{p,sc}$	$N_{p,sc}$	Battery pack	SC pack	
Baseline LFP pack	130	10	…	…	9.8	…	24.11
Optimized NMC pack	104	13	…	…	10	…	22.35 **(-7.3 %)**
Optimized NMC+SC pack	116	1	151	14	0.86	3.2	20.82 **(-13.6 %)**

compared to the baseline HEV [30], which uses an LFP battery pack of 9.8 kWh. The optimized NMC battery pack has, instead, an optimal energy capacity of 10 kWh. A properly designed ESS with an optimal power split strategy can reduce the fuel consumption without significantly increasing the energy capacity of the storage system. Fig. 10 shows the input velocity, required electrical power by the motors, electrical power from the genset, battery power, and battery SOC. Charge sustainability conditions are met and the fluctuations in power demand are handled mostly by the battery pack unless the battery power limit is reached. The zoomed plot in Fig. 10 shows that the genset provides a steady power whenever possible since frequent shifting in operating points causes the engine to consume more fuel.

In the right zoomed-in plot in Fig. 10, during a very high acceleration and deceleration, the battery pack reaches its maximum power limit. In this case, the genset provides the rest of the power to maintain the desired vehicle velocity. This behavior confirms that the optimal controller tries to maintain a steady engine operation to reduce fuel consumption as much as possible by using the battery power capacity to its allowable limit. The use of an HESS is motivated in that additional energy storage with high power capacity can handle the large power demand that might occur during driving.

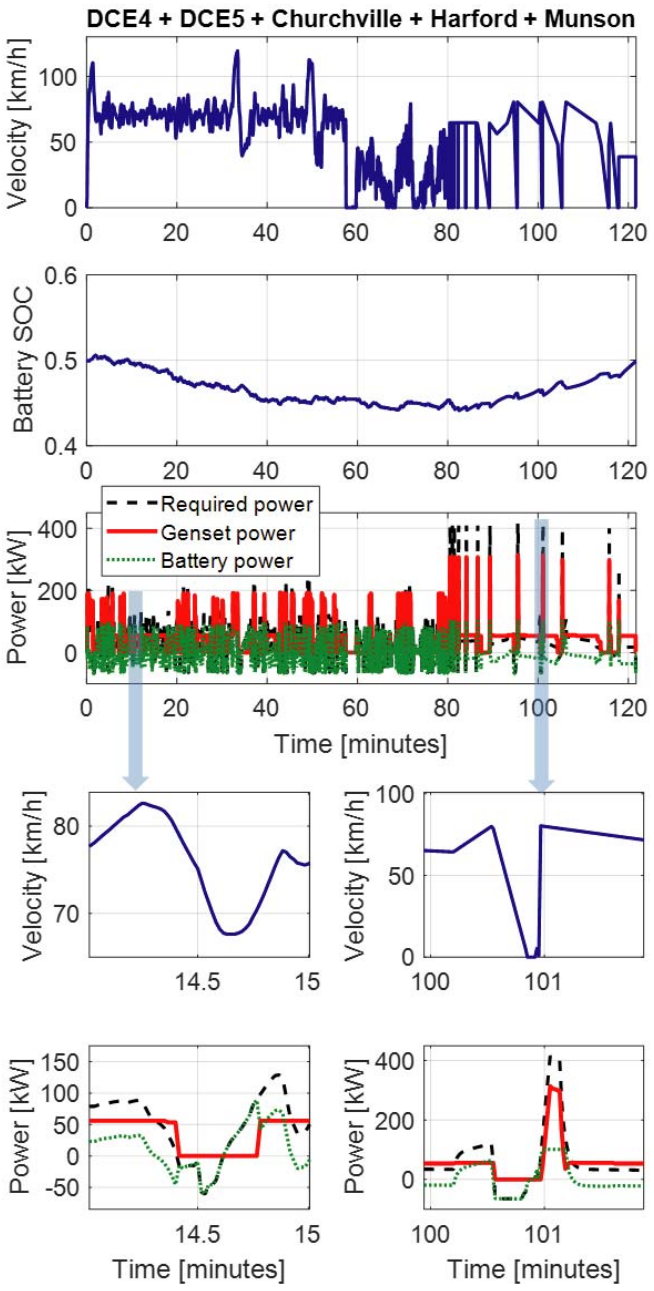

Fig. 10. Desired vehicle velocity, battery SOC, and power split decision between the genset and the battery pack for M-ATV with optimal NMC battery pack when simulating the concatenated drive cycle consisting of five military drive cycles.

B. HESS Configuration with NMC Li-Ion Battery and Supercapacitor

The design optimization framework using the HESS has five decision variables, three relating to the sizing of HESS itself and the other two relating to the PMP's costates. The number of battery cells in series is fixed and determined by dividing the power bus voltage (429 V) by the nominal cell voltage (3.7 V) of an NMC cell. The concatenated drive cycle is used to find the optimal size and power split decision for the HESS configuration. The optimal pack size, energy capacity, and fuel consumption are given in Table III. In the table, the fuel consumption results are also compared among the optimized HESS configuration, optimized NMC battery-only configuration, and baseline LFP battery-only configuration. The optimal HESS configuration reduces the fuel consumption for the concatenated cycle by 13.6% compared to the baseline. It is found that the energy capacity needed in the NMC battery pack is only 0.86 kWh, almost one-fourth smaller than the SC pack size. This indicates that the impact and role of the battery within the HESS are negligible. The SOC and C-rate profiles of the battery pack shown in Fig. 11 indicate that the battery pack is barely used, and the portion of the drive cycle requiring more participation from the battery is related to frequent start and stop instances and when high power is demanded by the vehicle during high acceleration.

Fig. 12 shows that the SC voltage fluctuates significantly due to frequent charge and discharge events and the SC can

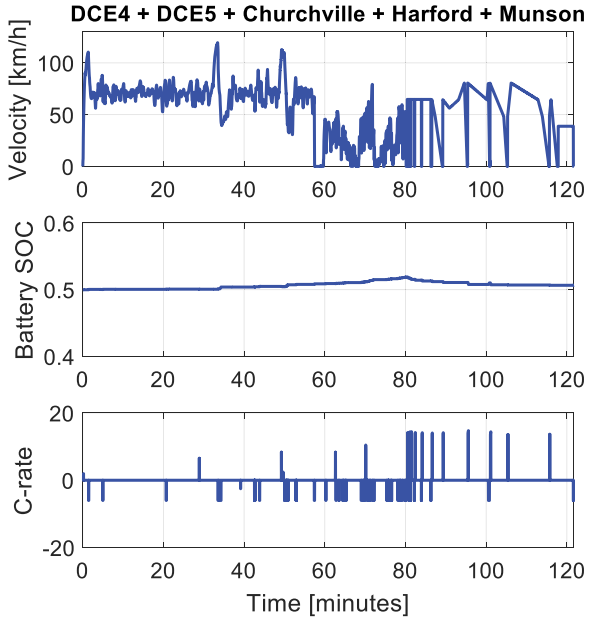

Fig. 11. Desired vehicle velocity, battery SOC, and C-rate for M-ATV with optimal HESS pack when simulating the concatenated drive cycle consisting of five military drive cycles.

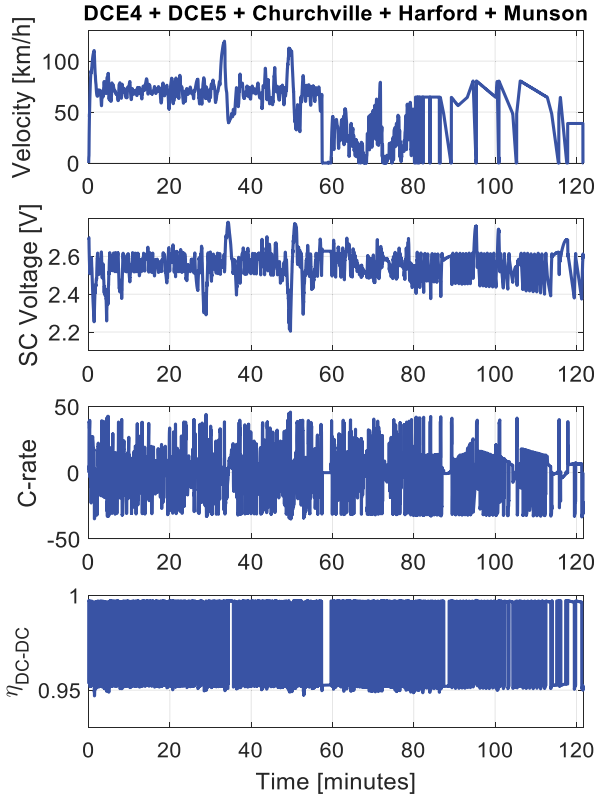

Fig. 12. Desired vehicle velocity, SC cell voltage, C-rate, and dc–dc converter efficiency for M-ATV with optimal HESS pack when simulating the concatenated drive cycle consisting of five military drive cycles.

take on high C-rate requests allowing the engine to be used as less as possible. The power loss in the dc–dc converter is also small during vehicle operation since the efficiency is maintained above 95% all the time. The C-rate and power

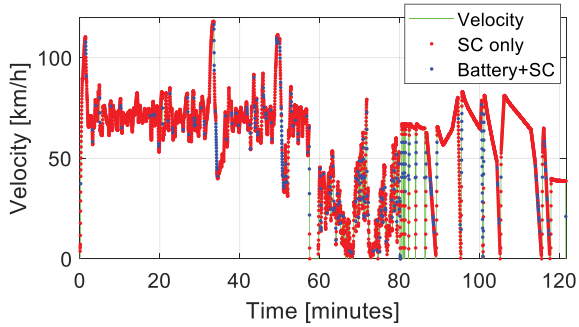

Fig. 13. Segmentation of the reference velocity profile into time instances when the vehicle uses only the SC and battery/SC together given the optimized HESS configuration.

from the SC are limited by the power limit imposed by the dc–dc converter.

In Fig. 13, the drive cycle is partitioned in regions that highlight the instances when the vehicle uses battery pack only, the SC only, and the battery/SC together. Fig. 13 shows that there is no instance when only the battery pack is used. In 91.1% of the time, the SC pack is used and the remaining 8.9% of the time, both the SC and the battery pack are used. The battery pack is only used during the high acceleration and deceleration event to supplement the SC. Fig. 14 shows the magnitude of the power from the genset, the battery pack, and the SC pack. The engine, the battery pack, and the SC pack power sum up to give the power requested by the in-hub motors to propel the vehicle. The charge and discharge power limits of the SC pack are limited by the dc–dc converter saturation limits, and the engine power is limited by the power limit of the genset. The PMP finds the optimal split of the engine power, battery power, and SC power allowing the engine to operate close to the brake-specific fuel consumption (BSFC) sweet spot. For the concatenated drive cycle used in this paper, a small NMC battery pack is selected by the optimization algorithm. However, the use of the small battery pack is also optimized to supplement the engine without violating the charge sustainability constraint. During high acceleration, some portion of the engine power is used to charge the SC pack. Fig. 15 shows that in both cases, i.e., optimized HESS and optimized battery-only configurations, the optimization algorithm ensures that the engine operation is forced on the optimal operating line. Moreover, when HESS is used, a lower average BSFC is obtained, thus confirming the initial results.

It is also visible from Fig. 14 that during braking, regenerative power mostly goes to the SC and occasionally to the battery. This behavior is due to the fact that the vehicle simulator is designed to charge the SC pack first and then the battery pack. Small battery pack utilization in Fig. 14 also indicates that SCs have the potential to be used as standalone energy storage for military vehicle hybridization.

The cost, weight, and volume of the HESS pack are additional factors to be considered for vehicle electrification. They can either be considered as additional optimization objectives or added as constraints based on the type, size, and functionality of the vehicle. Military vehicles have a

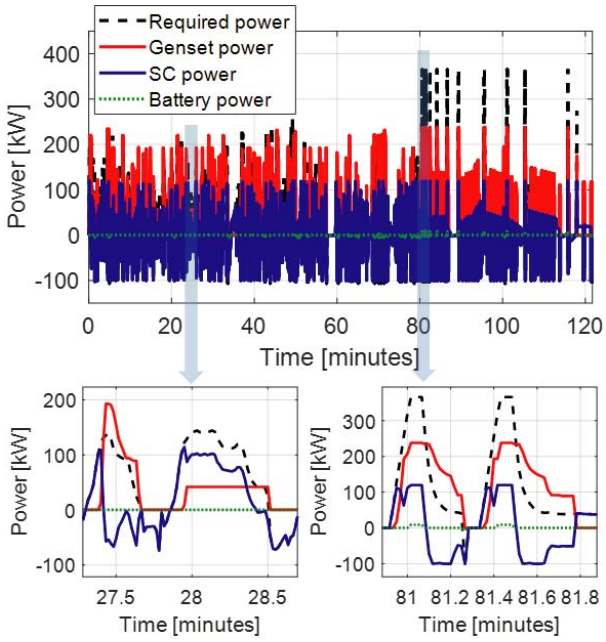

Fig. 14. Optimal power split among the genset, the battery pack, and the SC pack when simulating the series hybrid M-ATV simulator with an optimized HESS configuration for the concatenated drive cycle.

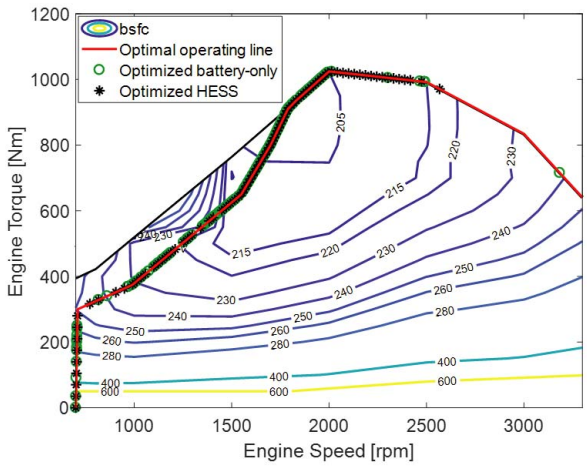

Average BSFC for the optimized battery-only configuration	128 g/kWh
Average BSFC for the optimized HESS configuration	90 g/kWh

Fig. 15. Engine operating points with the optimized battery-only and HESS configuration along with the engine BSFC contours for the concatenated cycle. The reduction in fuel consumption for HESS is obtained by shifting the engine operating points toward the more efficient region with a lower average BSFC.

higher degree of flexibility in design compared to commercial vehicles, and therefore, these factors are excluded from this paper. The proposed optimization algorithm is general enough to incorporate those factors and is currently intended to be considered in future studies.

Remark: In this paper, the current and voltage limits of a commercially available dc–dc converter were used. It is known that the physical limits of the converter impose a limit on the power delivered by the SC pack. A proper selection of the dc–dc converter through optimization or a customized dc–dc converter based on the vehicle power requirement could allow the SC to better utilize its available power capability.

V. Conclusion

This paper develops a novel mathematical framework for combined design optimization and optimal energy management of a series HEV with an HESS. The key element of the proposed framework is in the formulation of the Hamiltonian function, from the PMP strategy, to account for both time-varying control and design variables. The optimization framework is implemented to minimize fuel consumption of a notional military HEV by finding the optimal sizes the Li-ion and SC pack and optimal power split among the genset, battery pack, and the SC pack. The key findings of this paper are summarized below.

1) The simulation results show that for a concatenated drive cycle combining five military drive cycles, the optimal design and energy management algorithm can reduce the fuel consumption by nearly 7.3% for the battery-only case compared to the baseline.
2) When using the HESS configuration fuel consumption is reduced by up to 13% compared to the baseline.
3) The optimal pack size of the HESS configuration shows that the contribution of Li-ion battery pack is not significant if there is a properly sized SC available in the HESS configuration. Therefore, there is a high potential for using SCs for military vehicle hybridization even as a standalone storage system.

The future work aims at extending the proposed optimization algorithm to tackle multiple objectives such as battery health degradation, the lifecycle cost of the ESS. Active temperature control of the battery pack to prevent thermal runway and temperature related aging effects is also a part of the future work as well as the extension of the proposed framework to PHEVs and electric vehicles.

Disclaimer

Unclassified. DISTRIBUTION STATEMENT A. Approved for public release; distribution is unlimited.

Reference herein to any specific commercial company, product, process, or service by trade name, trademark, manufacturer, or otherwise does not necessarily constitute or imply its endorsement, recommendation, or favoring by the United States Government or the Dept. of the Army (DoA). The opinions of the authors expressed herein do not necessarily state or reflect those of the United States Government or the DoD, and shall not be used for advertising or product endorsement purposes.

References

[1] Z. Filipi *et al.*, "Engine-in-the-loop testing for evaluating hybrid propulsion concepts and transient emissions—HMMWV case study," *SAE Trans.*, vol. 115, pp. 23–41, Jan. 2006.
[2] D. M. Kramer and G. G. Parker, "Current state of military hybrid vehicle development," *Int. J. Electr. Hybrid Vehicles*, vol. 3, no. 4, pp. 369–387, 2011.

[3] D. M. Rizzo, "Military vehicle optimization and control," M.S. thesis, Dept. Mech. Eng.-Eng. Mech., Michigan Technol. Univ., Houghton, MI, USA, 2014.
[4] J. Li *et al.*, "Toward low-cost, high-energy density, and high-power density lithium-ion batteries," *J. Minerals, Met. Mater. Soc.*, vol. 69, no. 9, pp. 1484–1496, 2017.
[5] A. Santucci, A. Sorniotti, and C. Lekakou, "Power split strategies for hybrid energy storage systems for vehicular applications," *J. Power Sour.*, vol. 258, pp. 395–407, Jul. 2014.
[6] Z. Song *et al.*, "Multi-objective optimization of a semi-active battery/supercapacitor energy storage system for electric vehicles," *Appl. Energy*, vol. 135, pp. 212–224, Dec. 2014.
[7] J. Cao and A. Emadi, "A new battery/ultracapacitor hybrid energy storage system for electric, hybrid, and plug-in hybrid electric vehicles," *IEEE Trans. Power Electron.*, vol. 27, no. 1, pp. 122–132, Jan. 2012.
[8] A. Barré, F. Suard, M. Gérard, and D. Riu, "Electric vehicles performance estimation through a patterns extraction and classification methodology," *J. Power Sources*, vol. 273, pp. 670–679, Jan. 2015.
[9] Z. Liu, S. Onori, and A. Ivanco, "Synthesis and experimental validation of battery aging test profiles based on real-world duty cycles for 48-V mild hybrid vehicles," *IEEE Trans. Veh. Technol.*, vol. 66, no. 10, pp. 8702–8709, Oct. 2017.
[10] Z. Song, H. Hofmann, J. Li, X. Han, and M. Ouyang, "Optimization for a hybrid energy storage system in electric vehicles using dynamic programing approach," *Appl. Energy*, vol. 139, pp. 151–162, Feb. 2015.
[11] E. Schaltz, A. Khaligh, and P. O. Rasmussen, "Influence of battery/ultracapacitor energy-storage sizing on battery lifetime in a fuel cell hybrid electric vehicle," *IEEE Trans. Veh. Technol.*, vol. 58, no. 8, pp. 3882–3891, Oct. 2009.
[12] O. Erdinc and M. Uzunoglu, "Optimum design of hybrid renewable energy systems: Overview of different approaches," *Renew. Sustain. Energy Rev.*, vol. 16, no. 3, pp. 1412–1425, 2012.
[13] S. M. Lukic, S. G. Wirasingha, F. Rodriguez, J. Cao, and A. Emadi, "Power management of an ultracapacitor/battery hybrid energy storage system in an HEV," in *Proc. IEEE Vehicle Power Propuls. Conf. (VPPC)*, Sep. 2006, pp. 1–6.
[14] Z. Song, J. Hou, H. Hofmann, J. Li, and M. Ouyang, "Sliding-mode and Lyapunov function-based control for battery/supercapacitor hybrid energy storage system used in electric vehicles," *Energy*, vol. 122, pp. 601–612, Mar. 2017.
[15] P. Thounthong, S. Raël, and B. Davat, "Energy management of fuel cell/battery/supercapacitor hybrid power source for vehicle applications," *J. Power Sour.*, vol. 193, no. 1, pp. 376–385, 2009.
[16] M. Zolot, "Dual-source energy storage-control and performance advantages in advanced vehicles," in *Proc. 20th Electr. Vehicle Symp.*, 2003.
[17] Z. Yu, D. Zinger, and A. Bose, "An innovative optimal power allocation strategy for fuel cell, battery and supercapacitor hybrid electric vehicle," *J. Power Sources*, vol. 196, no. 4, pp. 2351–2359, 2011.
[18] A. Mirhoseini and F. Koushanfar, "HypoEnergy. Hybrid supercapacitor-battery power-supply optimization for energy efficiency," in *Proc. Design, Automat. Test Eur. Conf. Exhib. (DATE)*, Mar. 2011, pp. 1–4.
[19] E. Vinot and R. Trigui, "Optimal energy management of HEVs with hybrid storage system," *Energy Convers. Manage.*, vol. 76, pp. 437–452, Dec. 2013.
[20] A. Nguyen, J. Lauber, and M. Dambrine, "Optimal control based algorithms for energy management of automotive power systems with battery/supercapacitor storage devices," *Energy Convers. Manage.*, vol. 87, pp. 410–420, Nov. 2014.
[21] S. Zhang, R. Xiong, and F. Sun, "Model predictive control for power management in a plug-in hybrid electric vehicle with a hybrid energy storage system," *Appl. Energy*, vol. 185, pp. 1654–1662, Jan. 2017.
[22] S. Onori and L. Tribioli, "Adaptive pontryagin's minimum principle supervisory controller design for the plug-in hybrid GM chevrolet volt," *Appl. Energy*, vol. 147, pp. 224–234, Jun. 2015.
[23] M. Jain, C. Desai, and S. S. Williamson, "Genetic algorithm based optimal powertrain component sizing and control strategy design for a fuel cell hybrid electric bus," in *Proc. IEEE Veh. Power Propuls. Conf.*, Sep. 2009, pp. 980–985.
[24] M. Masih-Tehrani, M.-R. Ha'iri-Yazdi, V. Esfahanian, and A. Safaei, "Optimum sizing and optimum energy management of a hybrid energy storage system for lithium battery life improvement," *J. Power Sources*, vol. 244, pp. 2–10, Dec. 2013.
[25] X. Hu, N. Murgovski, L. M. Johannesson, and B. Egardt, "Comparison of three electrochemical energy buffers applied to a hybrid bus powertrain with simultaneous optimal sizing and energy management," *IEEE Trans. Intell. Transp. Syst.*, vol. 15, no. 3, pp. 1193–1205, Jun. 2014.
[26] X. Hu, L. Johannesson, N. Murgovski, and B. Egardt, "Longevity-conscious dimensioning and power management of the hybrid energy storage system in a fuel cell hybrid electric bus," *Appl. Energy*, vol. 137, pp. 913–924, Jan. 2015.
[27] T. Donateo, L. Serrao, and G. Rizzoni, "A two-step optimisation method for the preliminary design of a hybrid electric vehicle," *Int. J. Electr. Hybrid Vehicles*, vol. 1, no. 2, pp. 142–165, 2008.
[28] O. P. Sharma, S. Onori, and Y. Guezennec, "Analysis of Pontryagin's minimum principle-based energy management strategy for PHEV applications," in *Proc. ASME 5th Annu. Dyn. Syst. Control Conf., Joint JSME 11th Motion Vib. Conf.*, 2012, pp. 145–150.
[29] *Multi-Mission Family of Vehicles M-ATV*, Oshkosh Defense, Temecula, CA, USA, 2016.
[30] Y. Kim, A. Salvi, J. B. Siegel, Z. S. Filipi, A. G. Stefanopoulou, and T. Ersal, "Hardware-in-the-loop validation of a power management strategy for hybrid powertrains," *Control Eng. Pract.*, vol. 29, pp. 277–286, Aug. 2014.
[31] Z. Liu, A. Mamun, and S. Onori, "Combined battery design optimization and energy management of a series hybrid military truck," *SAE Int. J. Altern. Powertrains*, to be published.
[32] X. Lin *et al.*, "A lumped-parameter electro-thermal model for cylindrical batteries," *J. Power Sour.*, vol. 257, pp. 1–11, Jul. 2014.
[33] S. Fiorenti, J. Guanetti, Y. Guezennec, and S. Onori, "Modeling and experimental validation of a hybridized energy storage system for automotive applications," *J. Power Sour.*, vol. 241, pp. 112–120, Nov. 2013.
[34] Maxwell Technologies. *Datasheet-K2 Ultracapacitors*. [Online]. Available: http://www.maxwell.com/images/documents/K2Series_DS_1015370_5_20141104.pdf
[35] R. W. Erikson and D. Maksimovic, *Fundamentals of Power Electronics*. Norwell, MA, USA: Kluwer, 2001.
[36] J. Shen and A. Khaligh, "A supervisory energy management control strategy in a battery/ultracapacitor hybrid energy storage system," *IEEE Trans. Transport. Electrific.*, vol. 1, no. 3, pp. 223–231, Oct. 2015.
[37] *SINAMICS DCP—The Innovative DC–DC Converter for Industry and the Smart Grid*, Siemens Ind. Inc., Munich, Germany, 2016.
[38] R. W. Erickson, "DC–DC power converters," in *Wiley Encyclopedia of Electrical and Electronics Engineering*, vol. 1. Hoboken, NJ, USA: Wiley, 2001, no. 1, pp. 1–19.
[39] S. Onori, L. Serrao, and G. Rizzoni, *Hybrid Electric Vehicles: Energy Management Strategies*. London, U.K.: Springer, 2016.
[40] R. Hassan, B. Cohanim, O. de Weck, and G. Venter, "A comparison of particle swarm optimization and the genetic algorithm," in *Proc. 46th AIAA/ASME/ASCE/AHS/ASC Struct., Struct. Dyn. Mater. Conf.*, 2005, p. 1897.
[41] *Vehicle Test Facilities*, Aberdeen Test Center, Yuma Test Center, Aberdeen, MD, USA, 1995.

Abdullah-Al Mamun received the B.Sc. and M.Sc. degrees from the Department of Industrial and Production Engineering, Bangladesh University of Engineering and Technology, Dhaka, Bangladesh, in 2009 and 2011, respectively, and the Ph.D. degree from the Department of Mechanical Engineering, Pennsylvania State University, State College, PA, USA, in 2017.

He is currently a Post-Doctoral Fellow with the Department of Automotive Engineering, Clemson University, Greenville, SC, USA. His current research interests include lithium-ion battery modeling and control, hybrid vehicle design and energy management, physics-based modeling, and control of three-way catalyst.

Zifan Liu received the B.S. degree in automotive engineering from Jilin University, Changchun, China, in 2012, and the Ph.D. degree in automotive engineering from Clemson University, Greenville, SC, USA, in 2016.

From 2017 to 2018, he was a Post-Doctoral Fellow with the Clemson University International Center for Automotive Research, Greenville, SC, USA. He is currently an Engineer with Bosch Rexroth, Fountain Inn, SC, USA. His current research interests include population naturalistic driving data analysis, dynamics modeling, optimal design and control.

Denise M. Rizzo received the Ph.D. degree from Michigan Technological University, Houghton, MI, USA, in 2014.

From 2000 to 2008, she was a Controls Research and Development Engineer with Chrysler LLC, Auburn Hills, MI, USA. In 2008, she joined the U.S. Army Tank Automotive Research, Development, and Engineering Center, Warren, MI, USA, where she is currently a Senior Research Mechanical Engineer with the Powertrain Modeling and Simulation Team. She specializes in modeling, simulation, and control of propulsion systems of ground vehicles. She has authored or co-authored 15 articles in archival journals, 29 papers in refereed conference proceedings, and 4 technical government reports. She holds two patents.

Simona Onori (SM'15) received the Laurea degree (*summa cum laude)* in computer science engineering from the University of Rome Tor Vergata, Rome, Italy, in 2003, the M.S. degree in electrical and computer engineering from the University of New Mexico, Albuquerque, NM, USA, in 2004, and the Ph.D. degree in control engineering from the University of Rome Tor Vergata, in 2007.

Since 2017, she has been an Assistant Professor with the Energy Resources Engineering Department, Stanford University, Stanford, CA, USA.

Dr. Onori was a recipient of the SAE Ralph R. Teetor Educational Award, the 2017 NSF CAREER Award, the 2017 Clemson University College of Engineering and Science Dean's Faculty Fellows Award, the 2017 Clemson University Esin Gulari Leadership and Service Award, the 2016 Energy Leadership Award in the category Emerging Leader (for the Carolinas), and the 2015 Innovision Award (SC, USA).